

Atomic-scale Deformation Kinematics for Bicrystal Grain Boundaries under Shear Loading

G.J. Tucker¹, D.L. McDowell¹, and J.A. Zimmerman²*

¹ *Georgia Institute of Technology, Atlanta, USA;* ² *Sandia National Laboratories, Livermore, USA;*

Abstract

This research utilizes a method for calculating an atomic-scale deformation gradient within the framework of continuum mechanics using atomistic simulations to examine bicrystal grain boundaries subjected to shear loading. We calculate the deformation gradient, its rotation tensor from polar decomposition, and estimates of lattice curvature and vorticity for thin equilibrium bicrystal geometries deformed at low temperature. These simulations reveal pronounced deformation fields that exist in small regions surrounding the grain boundary, and demonstrate the influence of interfacial structure on mechanical behavior for the thin models investigated. Our results also show that more profound insight is gained concerning inelastic grain boundary phenomena by analyzing the deformed structures with regard to these continuum mechanical metrics.

1.0 Motivation

Engineered materials with nanometer-scale grain sizes have received significant interest recently because of their potentially enhanced material properties stemming from dominance of mechanisms involving intergranular dislocation nucleation and absorption, as well as coordinated atomic shuffling. However, a lack of knowledge and insight into these inelastic deformation mechanisms responsible for the observed improvements fuels further interest by the scientific community [1, 2]. As grain size approaches the nanometer scale, more atoms are located at or near grain boundaries and triple junctions, and the influence of these regions on material behavior increases accordingly. Recent research has supported the idea of a transition of deformation mechanisms with reduction in grain size, and that grain boundaries and triple junctions play a key role in these mechanisms [3-6].

Because the origins of material behavior are found at the atomic length scale, many efforts have sought to discover key structure-property relationships by investigating nanoscale dislocation phenomena. Experimental investigations into these issues are fraught with difficulty and uncertainty, so attention has turned to alternative methods such as computer modeling to gain insight. It is important to note that the eventual cooperative effects of these nanoscale deformation mechanisms leading to material failure, is inherently multiscale. Thus, recent modeling efforts have focused on bridging both length and time scales to

* Correspondence: garritt.tucker@gatech.edu

understand the influence of structural features on material plasticity. However, there seems to be an inherent disconnect between larger spatial scale continuum or statistical models and the underlying discrete nature of these nanoscale deformation mechanisms. Accordingly, it is necessary to complement such large scale models with nanoscale information such as insight into various inelastic deformation mechanisms from atomistic simulations. Bridging scales by using atomistics to inform continuum models is an area of great importance in multiscale modeling and design of deformation- and fracture-resistant materials.

This paper presents methods for calculating continuum mechanical quantities related to lattice deformation characteristics within an atomistic framework. Two-dimensional bicrystalline structures will be used to analyze the shear deformation response in terms of these continuum mechanical metrics, focusing on deformation fields in regions at or near each grain boundary. There is a direct correlation between atomic grain boundary structure and shear deformation mechanism in each 2D structure, and that each mechanism leads to a unique deformation field that is analyzed using the formulated continuum metrics.

2.0 Mathematical Background

Continuum mechanical concepts such as the deformation gradient, \mathbf{F} , rotation tensor, \mathbf{R} , velocity gradient, \mathbf{L} , and vorticity, \mathbf{W} , are formulated in the context of an atomistic framework and utilized for investigating the shear deformation behavior of 2D bicrystalline structures. Zimmerman *et al.* [7] formulated the deformation mapping $\mathbf{F} = \partial\mathbf{x}/\partial\mathbf{X}$ in an atomistic framework using the interatomic spacing of an atom α and its nearest neighbor β for an estimate of atomic strain, using a locally affine assumption

$$x_i^{\alpha\beta} = F_{iI} X_I^{\alpha\beta} \quad (1)$$

By minimizing the least squares error associated with \mathbf{F} as computed with respect to all nearest neighbors, an appropriate value for \mathbf{F} is obtained for a particular atom α according to

$$F_{iI}^\alpha = \omega_{iM}^\alpha \left(\eta_M^\alpha \right)_{MI}^{-1} \quad (2)$$

where both ω and η are defined as

$$\omega_{iM}^\alpha \equiv \sum_{\beta=1}^n x_i^{\alpha\beta} X_M^{\alpha\beta} \quad \text{and} \quad \eta_M^\alpha \equiv \sum_{\beta=1}^n X_I^{\alpha\beta} X_M^{\alpha\beta} \quad (3)$$

This formulation provides a definition of the deformation gradient for each atom α based on the nearest neighbor list associated with the reference configuration. Additional continuum mechanical quantities as previously mentioned can now be formulated within an atomistic framework based on this description.

3.0 Computational Setup

The 2D bicrystal structures were generated containing a symmetric tilt grain boundary located at the center of the simulation domain with the boundary plane normal vector in the vertical direction, as shown in Fig. 1. Periodic boundary conditions were employed on surfaces normal to the x-direction, and constrained free surfaces were enforced in the vertical direction on the upper and lower surfaces of the periodic unit cell. A conjugate gradient energy minimization method in LAMMPS [8] was used to obtain the initial grain boundary structures with an energy convergence of 10^{-25} , and all grain boundaries were then equilibrated for 10 ps before undergoing shear deformation at 10K, consistent with the NVE ensemble. A shifted Lennard-Jones interatomic pair potential based on a lattice parameter of 4.08 Å was used and designed so that both the potential energy and its first derivative are zero at the cutoff radius; the energy is zero at any radius greater than the cutoff value. The key potential parameters are the cutoff radius (7.6364 Å) which includes the first and second neighbor shells only, the cohesive energy (-3.93 eV), mass (196.97 amu), σ (3.63638 Å) and ϵ (1.5726 eV). The L-J potential was employed for model 2D problems for qualitative purposes rather than for quantitative agreement of dislocation mechanisms that might be achieved in 3D simulations using EAM potentials, for example.

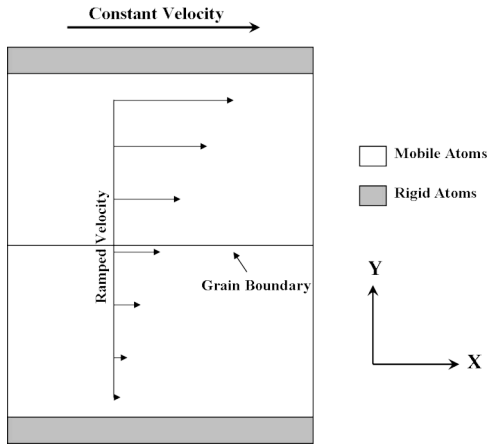


Figure 1: Schematic showing a general grain boundary structure and simulation constraints necessary for the applied shear deformation.

An additional constraint necessary for shear is that atoms located within three times the potential cutoff distance of both the top and bottom surfaces were 'frozen' and held fixed in their perfect lattice positions throughout the simulation. Shear deformation was applied to each structure by holding the bottom group completely fixed from movement in all directions, and applying a constant velocity in the x-direction to the top region. Due to inherent high strain rate conditions of molecular dynamics (MD), a ramped velocity field was also imposed on all atoms between the two rigid regions. This condition prevents

possible shock wave generation in the structure from the prescribed velocity of the top atomic region [9]. The prescribed velocity on the top region corresponds to an approximate shear strain rate of 10^8 s⁻¹, and the shear strain is given by $\gamma = \arctan(l/d_o)$, where l is the shear displacement and d_o is the height between the top and bottom frozen atomic regions.

4.0 Mathematical Formulation

In addition to \mathbf{F} , continuum measures of \mathbf{R} , \mathbf{L} , and \mathbf{W} were also formulated within an atomistic framework. Once \mathbf{F} is known based on the nearest neighbor list, its multiplicative decomposition into a rotation tensor \mathbf{R} and stretch tensor \mathbf{U} is straightforward.

$$\mathbf{F} = \mathbf{R}\mathbf{U} \quad (4)$$

From there, \mathbf{R} is separated into both symmetric and skew-symmetric components, and as with any skew-symmetric tensor, taking the skew-symmetric component of \mathbf{R} we define an axial vector also known as the microrotation vector, $\boldsymbol{\varphi}$.

$$\varphi_k = -\frac{1}{2} \epsilon_{ijk} (R_{skew})_{ij} \quad (5)$$

where ϵ_{ijk} is the permutation tensor. Another important continuum concept is vorticity, which is derived from the calculation of the velocity gradient, \mathbf{L} . In our formulation, we use the instantaneous atomic velocities to approximate \mathbf{L} .

$$\mathbf{L} = \frac{\partial \mathbf{v}}{\partial \mathbf{x}} \quad (6)$$

From this description, an atomic definition of \mathbf{L} can be formulated in a similar manner to the formulation of \mathbf{F} for each individual atom, α . Beginning with Eq. (6) and forming a summation over the squared differences, we get

$$C_i^\alpha = \sum_{\beta=1}^n (v_i^{\alpha\beta} - L_{ik}^\alpha x_k^{\alpha\beta})^2 \quad (7)$$

then minimize C^α by some choice of L^α :

$$\sum_{\beta=1}^n (v_i^{\alpha\beta} x_l^{\alpha\beta} - L_{ik}^\alpha x_k^{\alpha\beta} x_l^{\alpha\beta}) = 0 \quad (8)$$

This equation is rearranged and simplified to become

$$\rho_{il}^\alpha = L_{ik}^\alpha \tau_{kl}^\alpha \quad (9)$$

where

$$\rho_{il}^\alpha = \sum_{\beta=1}^n v_i^{\alpha\beta} x_l^{\alpha\beta} \quad \text{and} \quad \tau_{kl}^\alpha = \sum_{\beta=1}^n x_k^{\alpha\beta} x_l^{\alpha\beta} \quad (10)$$

Once these substitutions are made, Eq. (9) is rewritten as

$$L_{ik}^\alpha = \rho_{il}^\alpha (\tau^\alpha)_k^l \quad (11)$$

this is now the atomic formulation of the velocity gradient for each atom α depending on all nearest neighbors β .

The vorticity or spin tensor \mathbf{W} is the skew-symmetric component of \mathbf{L} and is derived from the additive decomposition of \mathbf{L} .

$$\mathbf{L} = \mathbf{D} + \mathbf{W} \quad (12)$$

Where \mathbf{D} is the rate of deformation tensor and \mathbf{W} is the spin or vorticity tensor. The calculation of the vorticity vector ($\boldsymbol{\omega}$) from \mathbf{W} is identical to the method used to determine $\boldsymbol{\phi}$, i.e.,

$$\omega_k = -\frac{1}{2} \epsilon_{ijk} W_{ij} \quad (13)$$

5.0 Results

Consider the shear deformation behavior of three 2D grain boundary structures with a common tilt axis and different disorientation angle (Ψ) values. Each grain boundary structure is approximately 300 \AA^2 in total area, and three different Ψ values are used: 9.4° , 15.2° , and 27.8° . These three different disorientation angle values were chosen because each boundary structure displayed a different deformation mechanism under applied shear. The three different mechanisms are grain boundary migration, sliding, and dissociation respectively. Images of the initial grain boundary structures after energy minimization and at approximately 5% shear strain are shown below in Fig. (2) and are colored with respect to potential energy.

It is obvious from Fig. (2) that each boundary exhibits a different deformation mechanism. There is an inherent connection between grain boundary structure and deformation behavior under shear. This does not imply that each grain boundary structure within this misorientation range will display a unique deformation mechanism, but that atomic grain boundary structure influences mechanical response. It is possible that other shear deformation mechanisms exist

within this misorientation range; however, it is more likely that additional boundaries within this misorientation range would display some varying combination of the aforementioned mechanisms based on the atomic structural composition in addition to other factors.

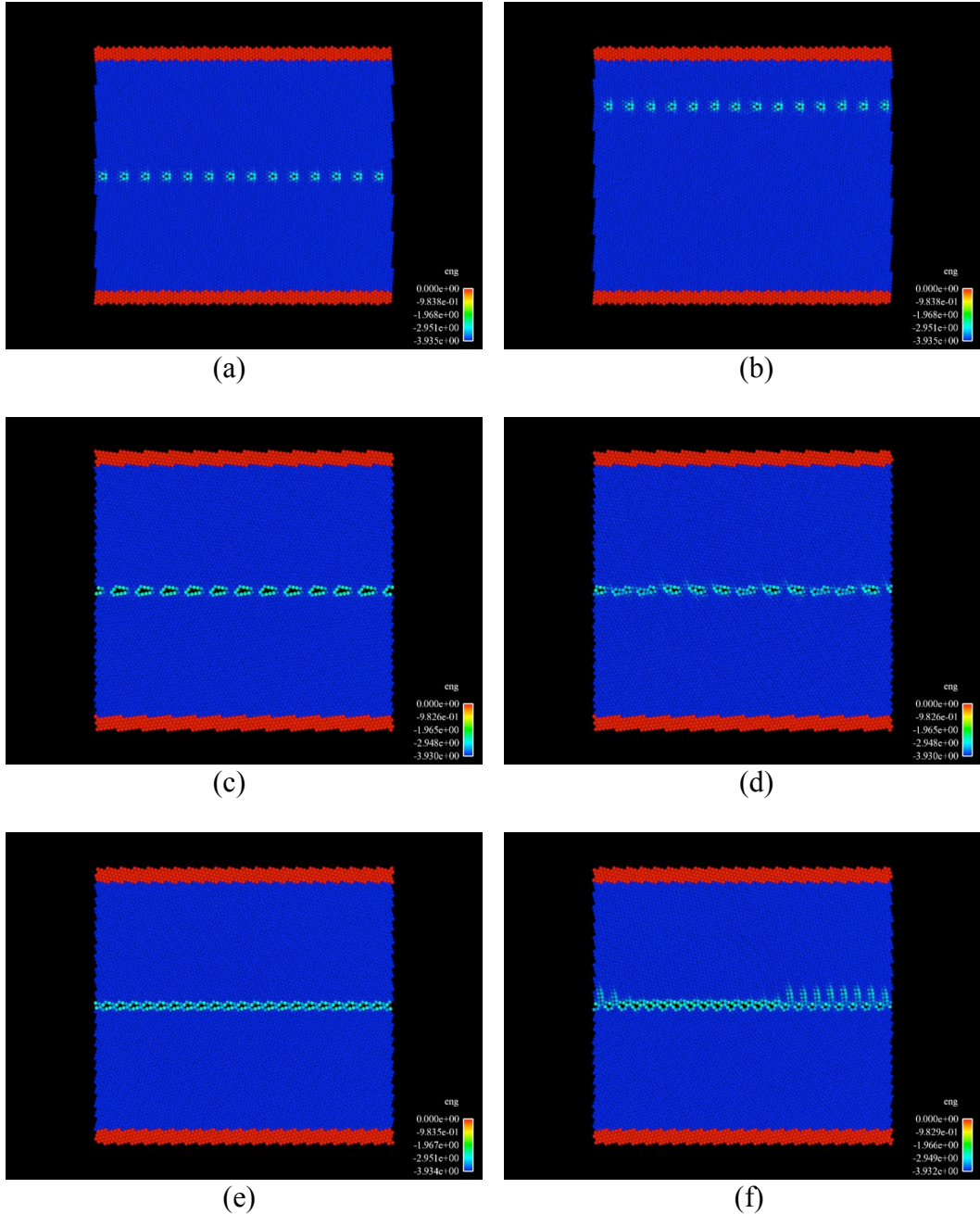


Figure 2: Initial 2D grain boundary structures (a), (c), (e), and those same boundaries at approximately 5% shear strain (b), (d), and (f), respectively.

To further investigate the shear deformation response of these grain boundary structures, continuum mechanical quantities such as \mathbf{F} , \mathbf{R} , \mathbf{L} , and \mathbf{W} were

employed. The grain boundary sliding mechanism produces negligible deformation in the surrounding lattice regions and is highly localized to the boundary region. Therefore, explicit consideration of this mechanism and continuum mechanical treatments of it are not considered here. This analysis will cover both the migration and dissociation mechanisms simultaneously. Brief discussions of the calculated atomic level \mathbf{F} , \mathbf{R} , φ , and ω values will follow, and significant results for each quantity will be highlighted.

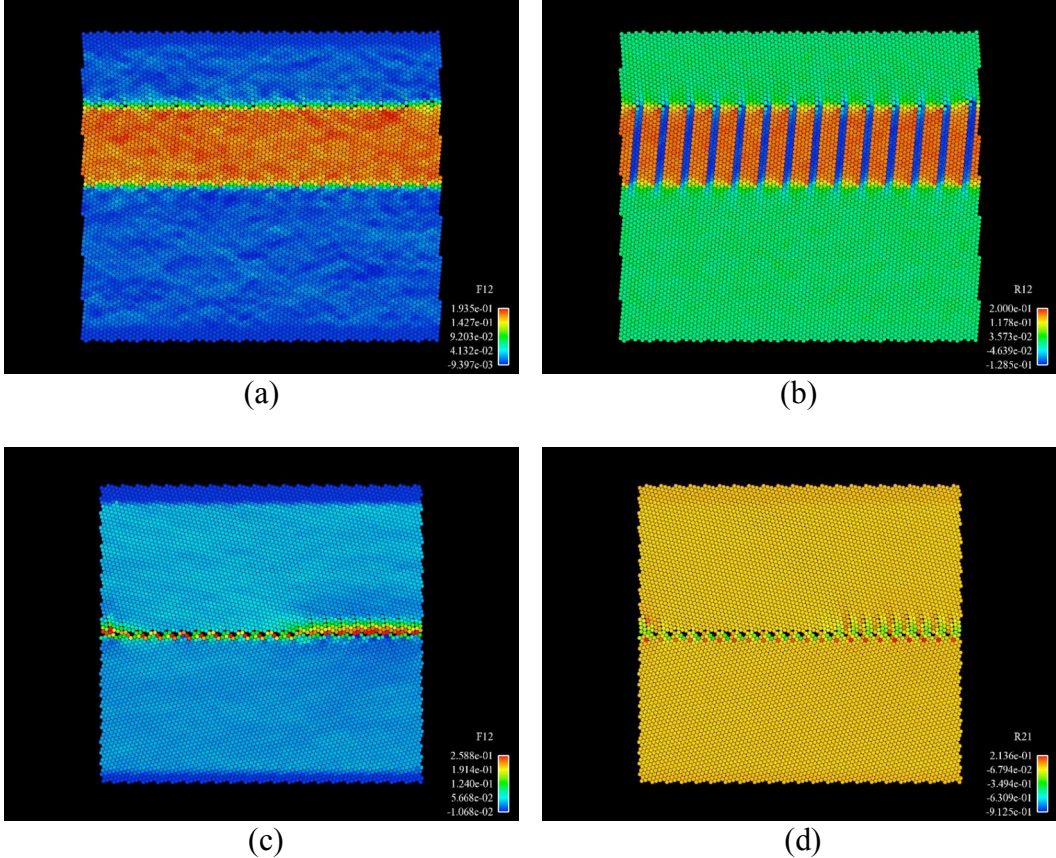


Figure 3: At approximately 5% shear strain, the calculated F_{12} (a) and R_{12} (b) components for each atom during grain boundary migration are shown along with the F_{12} (c) and R_{21} (d) components during grain boundary dissociation.

The components of the deformation gradient and its rotation tensor provide information about the influence of specific directions on atomic deformation. In Fig. (3a), a relatively uniform deformation field is shown that highlights the lattice region that underwent deformation as a consequence of the boundary migration in the vertical direction (x_2). This region is without large contrasts in this component because there is very little difference in the dependence of the horizontal direction (x_1) of atomic position in the deformed configuration on the x_2 component in the initial configuration. Fig. (3b) is colored according to R_{12} values for the migration mechanism. One thing to note is that as the grain

boundary migrates, the orientation of the upper lattice region traversed by the migrating boundary reorients to an orientation identical to that of the lower lattice.

In Figs. (3c-d), more confined deformation is observed in the grain boundary dissociation mechanism than in migration, and a deformation region is produced at the boundary which encompasses the dissociated planes extending out from the boundary. As dissociation occurs, atoms located near the boundary experience a net deformation as a result of the applied shear deformation, and (d) shows a rotational component in the atomic deformation field for atoms located near the slipped planes. This mechanism is quite different than the migration mechanism because the atomic deformation accommodation is mainly due to sliding events between atoms with small atomic rotations around the slipped planes, whereas the migration mechanism is due to large collective atomic rotation. The dissociations that arise in this case are localized slipping events occurring between two planes with small rotation fields between, not large atomic region rotations as seen in the migration mechanism to accommodate the lattice mismatch as observed in (a-b) as the grain boundary migrates vertically.

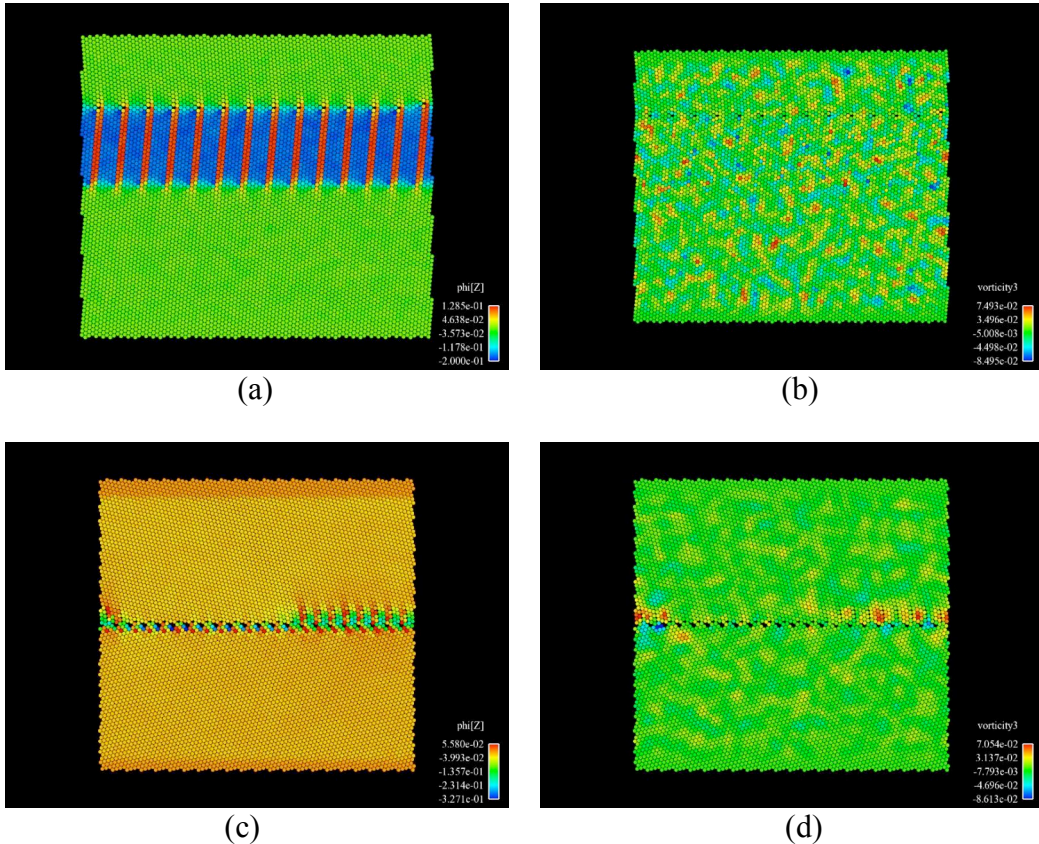


Figure 4: The calculated quantities of ϕ_3 and ω_3 are shown for each atom for both boundary migration (a-b) and dissociation (c-d) at 5% shear strain. Notice the difference in microrotation between the migration planes and lattice regions located between migration planes in (a), and the presence of noise in the vorticity images (b,d).

In addition to the valuable information obtained from analyzing the deformation fields with regard to \mathbf{F} and \mathbf{R} , further insight into the deformation field behavior can be obtained from atomic descriptions of φ and ω to estimate lattice curvature and vorticity. First consider the migration case shown in Fig. (4a-b). It is clear that the microrotation behavior of migration plane atoms is different from that of inter-region atoms not only in magnitude but direction, and large collective atomic rotation is present instead of small isolated rotation fields. All inter-region atoms possess an almost identical value of φ_3 near -0.2, and migration plane atoms display a similar trend and value of approximately 0.13. Fig. (4c) shows the microrotation of the dissociation mechanism, and it is clear that the direction of the atomic microrotation varies on opposing sides of each slip plane. This indicates that an atom's nearest neighbors undergo a small simultaneous rotation as dissociation occurs, but varies depending on the atom's location with regard to the slip plane.

Figs. (4b,d) shows the results of atomic vorticity calculations as outlined previously. It appears that no distinguishable vorticity fields exist in Fig. (4b) as a consequence of the migration mechanism. However, small localized domains of vorticity appear in the dissociation mechanism as shown in Fig. (4d) around the slip regions. One of the most obvious features of these figures is the presence of noise in the lattices and the lack of more distinguishable vorticity fields. This is a natural consequence of the proposed method for determining \mathbf{L} , and future work will explore alternative methods and elucidate the effect of these efforts on the calculated vorticity fields for each mechanism. Additionally, it is also quite possible that probing higher shear strains, larger simulation domains and thin 3D grain boundary structures will generate more interesting results concerning vorticity and lattice curvature fields.

6.0 Conclusions

This work has shown that continuum mechanical deformation quantities such as \mathbf{R} , \mathbf{L} , φ and ω can be formulated within an atomistic framework based on the description of \mathbf{F} , as provided in [7]. Additionally, the implementation of these descriptions can provide unique and fundamental insight into atomic phenomena occurring in deformation fields at or near grain boundaries at the origins of nanoscale plasticity events under applied shear. Examples of three different deformation mechanisms associated with three different grain boundary structures were shown, and detailed analysis was given for two mechanisms in the context of these continuum metrics. Each metric provided distinct information about local and neighboring atomic behavior during each mechanism. Varying atomic behaviors were seen in the context of each continuum quantity during shear deformation, and information about the extent of deformation away from the boundary was also shown to depend on the deformation mechanism.

Acknowledgements

G.J. Tucker is grateful for support of Sandia National Laboratories in a summer engineering intern program, as well as support of a NSF grant CMMI-0758265 on multiresolution, coarse-grained modeling of 3D dislocation nucleation and migration. D.L. McDowell is grateful for additional support of the Paden Chair in metals processing. Sandia is a multiprogram laboratory operated by Sandia Corporation, a Lockheed Martin Company, for the United States Department of Energy's National Nuclear Security Administration under contract DE-AC04-94AL85000.

References

- [1] D. L. McDowell, Materials design: A useful research focus for inelastic behavior of structural metals, *Theoretical and Applied Fracture Mechanics* 37 (2001) 245-259.
- [2] H. Van Swygenhoven, P. M. Derlet, and A. Hasnaoui, Atomistic modeling of strength of nanocrystalline metals, *Advanced Engineering Materials* 5 (2003) 345-50.
- [3] V. Randle, *The Role of the Coincident Site Lattice in Grain Boundary Engineering*, The University Press, Cambridge, 1996.
- [4] P. G. Sanders, J. A. Eastman, and J. R. Weertman, Elastic and tensile behavior of nanocrystalline copper and palladium, *Acta Materialia* 45 (1997) 4019-4025.
- [5] J. Schiotz, F. D. Di Tolla, and K. W. Jacobsen, Softening of nanocrystalline metals at very small grain sizes, *Nature* 391 (1998) 561-3.
- [6] D. Wolf, Structure-energy correlation for grain boundaries in f.c.c. metals. III. Symmetrical tilt boundaries, *Acta Metallurgica et Materialia* 38 (1990) 781-90.
- [7] J. A. Zimmerman, D. J. Bammann, and H. Gao, Deformation gradients for continuum mechanical analysis of atomistic simulations, *International Journal of Solids and Structures* (2008), In press.
- [8] S. Plimpton, Fast parallel algorithms for short-range molecular dynamics, *Journal of Computational Physics* 117 (1995) 1-19.
- [9] M. F. Horstemeyer, M. I. Baskes, V. C. Prantil, J. Philliber, and S. Vonderheide, A multiscale analysis of fixed-end simple shear using molecular dynamics, crystal plasticity, and a macroscopic internal state variable theory, *Modelling and Simulation in Materials Science and Engineering* 11 (2003) 265-86.